Electronic Supplementary Material (ESI) for Inorganic Chemistry Frontiers.

Supplementary Information

for

Stapled Ligand for Synthesis of Highly Emissive $CsPbBr_3$ Perovskite Nanocrystals in Polar Organic Solvent

Tianju Chen[a], Qi Yang[a], Peng Zhang[a], Ruihao Chen[*b], Yuke Lin[a], Weifang Zhou[a], Laizhi Sui[*c], Xuan Zheng[*a], Guoliang Chen[a], Feiming Li[*a]

[a]College of Chemistry, Chemical Engineering and Environment, Minnan Normal University, Zhangzhou, 363000, P.R. China

[b]State Key Laboratory of Solidification Processing, Center for Nano Energy Materials, School of Materials Science and Engineering, Northwestern Polytechnical University and Shaanxi Joint Labortary of Graphene, Xi'an 710072, P. R. China.

[c]State Key Laboratory of Molecular Reaction Dynamics and Dalian Coherent Light Source, Dalian Institute of Chemical Physics, Chinese Academy of Sciences, Dalian, 116023 China

[*]Email: lfm1914@mnnu.edu.cn, zx1974@mnnu.edu.cn, rhchen@nwpu.edu.cn, lzsui@dicp.ac.cn

Experimental section

Materials.

Cesium hydroxide (CsOH, 50wt% in water), cesium bromide (CsBr, 98%), lead bromide ($PbBr_2$, 99%), cesium carbonate (Cs_2CO_3, 99.9%), perfluoroglutaric acid (PFGA, 98%), perfluorovaleric acid (PFVA, 96%), perfluorosuccinic acid (PFSA, 97%), perfluoroadipic acid (PFAA, 98%), Oleic acid (OA, 90%) oleamine (OAm, 80%-90%), octadecylene (ODE, 90%) and dimethyl sulfoxide (DMSO, 99.7%, Extra Dry, with molecular sieves, Water$\leqslant$50 ppm) was purchased from Aladdin (Shanghai, China). Anhydrous ether (99.7%), toluene (99.5%), isopropyl alcohol (99.6%) and ethanol (99.5%) were purchased from Xinopharm Chemical Reagent Co., Ltd (Shanghai, China). All chemicals were used without further purifications.

Synthesis of cesium perfluoropglutarate (Cs_2PFGA) and other cesium carboxylate salts.

The Cs_2PFGA were synthesized through an acid-base neutralization reaction. Typically, 2.4 g PFGA were dissolved in 20 ml isopropyl alcohol and heated to 60 °C. After that, 1.6 ml 50wt% CsOH aqueous solution was dropwise added to the acid solution. Afterward, the resulting mixture was naturally crystallized at room temperature and purified twice via anhydrous ether. Finally, the product was obtained by vacuum-drying at 60 °C overnight and sealed in a centrifuge tube immediately. For the synthesis of CsPFVA/Cs_2PFSA/Cs_2PFAA, equimolar PFVA/PFSA/PFAA were used to replace the PFGA described above, and the others maintained the same as the synthesis of Cs_2PFGA.

Synthesis of the $CsPbBr_3$ NCs with PFGA/PFVA/PFSA/PFAA passivation.

The PFGA-$CsPbBr_3$ NCs were prepared by ligand-assisted precipitation method with some modifications.[1] Typically, 50.4 mg of Cs_2PFGA and 36.7 mg of $PbBr_2$ were predissolved in 1 ml of DMSO with sonication. Then, 1 ml of the precursor solution is added to 10 ml of ethanol under magnetic stirring at room temperature. After stirring for 15 min, the resulting PFGA-$CsPbBr_3$ NCs were separated and purified twice in

ethanol by centrifugation at 8000 rpm for 5 min before further characterization. For the synthesis of $CsPbBr_3$ NCs with PFVA/PFSA/PFAA passivation, the similar manner to PFGA-$CsPbBr_3$ NCs was operated except for altering Cs_2PFGA to equimolar CsPFVA/Cs_2PFSA/Cs_2PFAA.

Synthesis of the classic OA/OAm-$CsPbBr_3$ NCs by the Hot-Injection Method.

For comparison, OA/OAm-$CsPbBr_3$ NCs were prepared by a hot-injection method developed by Protesescu et al.[2] In order to synthesize cesium-oleate (Cs-OA), 0.16 g of Cs_2CO_3, 8 mL of ODE and 0.5 mL of OA were added in a three-neck flask and vacuum degassed for 1 h at 120 °C. Then, under N_2 atmosphere, the solution was heated to 140 °C to make all Cs_2CO_3 reacted completely and form Cs-OA solution. Next, for synthesis of OA/OAm-$CsPbBr_3$ NCs, 0.069 mg of $PbBr_2$ was loaded into a new three-neck flask with 5 ml ODE, 0.5 ml of OA and 0.5 ml of OAm, and then vacuum degassed for 1 h at 120 °C. After $PbBr_2$ being completely dissolved, the reactants were then heated to 160 °C under N_2 atmosphere. Afterward, 0.4 mL of the as-prepared Cs-OA solution was swiftly injected into system. 5 s later, the reaction mixture was cooled down by an ice-water bath. Finally, the OA/OAm-$CsPbBr_3$ NCs were purified with toluene by centrifugation at 10000 rpm and re-dispersed in toluene.

Fluorescence detection of Cl^- through PFGA-$CsPbBr_3$ NCs.

First, PFGA-$CsPbBr_3$ NCs was diluted with ethanol to an appropriate concentration through controlling absorption intensity to about 0.8 in their intrinsic absorption wavelength (335 nm). Then, a series of Cl^- standard solutions from 0 to 300 mM were prepared using NaCl and ultrapure water. Under 365 nm excitation, PL spectra versus the concentration of Cl^- were recorded by mixing 3 ml of PFGA-$CsPbBr_3$ NCs and 5 μl NaCl solutions, and the color change of the samples was collected under 365 nm UV lamp. The selectivity or actual sample detection of PFGA-$CsPbBr_3$ NCs to Cl^- was the same as the above. The actual samples are obtained from three healthy volunteers.

Characterization.

Fluorescence (PL) emission spectra were collected by a Gary Eclipse (Agilent, USA) spectrophotometer. Absolute PL quantum yields and were measured using a FLS 980 (Edinburgh, UK) spectrometer with a nanosecond flash lamp. Specord 200 plus (Analytik Jena, Germany) was employed to obtain the UV-Vis absorption spectra in transmission mode. The morphologies were investigated by Tecnai-G2-F30 (FEI, USA) transmission electron microscope instruments at 200 kV. The hydrodynamic diameter of the PNCs was collected by Dynamic Light Scattering (DLS) with a Zetasizer Nano ZS3600. Fourier-transform infrared spectroscopy (FTIR) spectra of the compounds are recorded on Nicolet IS 10 (Thermo Fisher, USA) on the range from 500 to 4000 cm^{-1}. X-ray diffraction (XRD) were obtained with an Ultima IV diffractometer (Rigaku, Japan) with Cu Kα (1.79 Å) over the 2θ range of 10-60°. X-ray photoelectron spectroscopy (XPS) spectra was conducted on the composite powder by an ESCALAB 250XI (Thermo Fisher, USA) using a monochromatic Al Kα X-ray source (1486.6 eV). Binding energies were corrected by the C 1s peak (set at 284.8 eV) of the sp3 hybridized (C-C) carbon.

The femtosecond transient absorption measurements were carried out on a homemade pump probe system coupled with a regeneratively amplified Ti:sapphire laser system (Coherent Legend Elite HE+USP-1K-III, 35 fs, 1 kHz). The 400 nm pump pulses were generated by focusing a part of fundamental light into a BBO crystal. The broadband probe pulses (white light continuum from 440 to 800 nm) were produced by focusing a small portion of the fundamental 800 nm laser pulses into a sapphire plate (3 mm). The delay between the pump and probe pulse was controlled by a motorized delay stage. The pump and probe beams overlapped spatially in the sample cell. After passing through the sample, the transmission changes of the probe light were detected by a fiber spectrometer (AvaSpec-ULS2048CL-EVO, Avantes).

Computation details.

The first-principles DFT calculations were performed in the CP2K 8.2 software package[3]. The Goedecker-Teter-Hutter (GTH) pseudopotential and double-zeta GTH-MOLOPT basis set was employed[4-5], and the Perdew-Burke-Ernzerhof (PBE)

functional of a generalized gradient approximation method was adopted to describe the exchange and correlation interaction[6]. The cut-off energies were set at 520 Ry. The 001 surface of $CsPbBr_3$ crystal was simulated by a (3*3) seven-slab model with the periodic boundary condition in the XY directions. A vacuum region of 20 Å was set to avoid the interaction between slabs. The Brillouin zone was only sampled at the Γ point due to the sufficient size of this model. The DFT-D3BJ method was also adopted to better describe the van der Waals interactions[7-8]. During these geometry optimizations, the bottom two atomic slayers were fixed to mimic the constrained environment in the actual solid phase, while the top five layers and the ligands were fully relaxed until reaching the default convergence thresholds, i.e., $3*10^{-3}$ and $1.5*10^{-3}$ Hartree for the maximum and RMS geometry change, $4.5*10^{-4}$ and $3*10^{-4}$ Hartree/Bohr for the maximum and RMS force, respectively. In addition, the self-consistent field (SCF) calculation was set with a convergence criterion of $3*10^{-6}$ Hartree.

Based on these optimized conformations, the binding energy of each ligand ($\Delta E_{binding}$) was calculated as follows:

$$\Delta E_{binding} = E_{ligand/surface} - E_{surface} - E_{ligand} \quad (1)$$

Wherein, $E_{surface}$, E_{ligand}, and $E_{ligand/surface}$ are the energies of the (001) surface, ligand, and the surface with carboxylate ligand, respectively. During the calculation process, the basis set superposition error (BSSE) was also considered to correct the binding energy[9].

Supplemented Figures

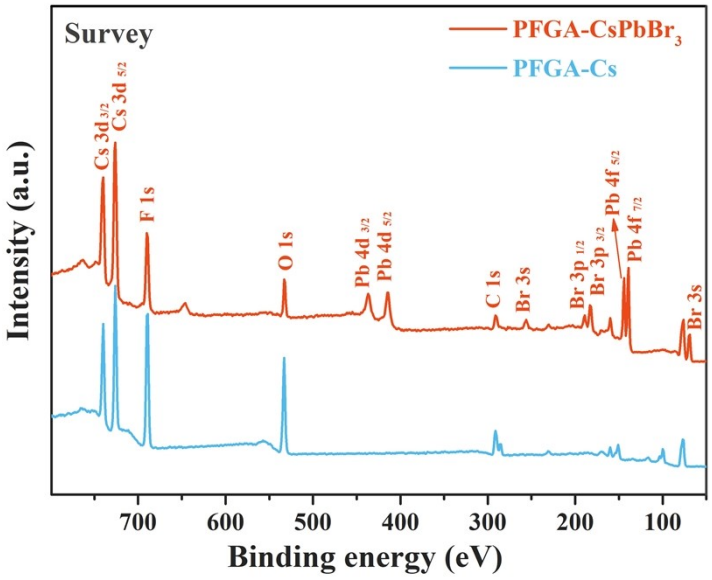

Figure S1. Full-scan XPS spectrum of PFGA-$CsPbBr_3$ NCs.

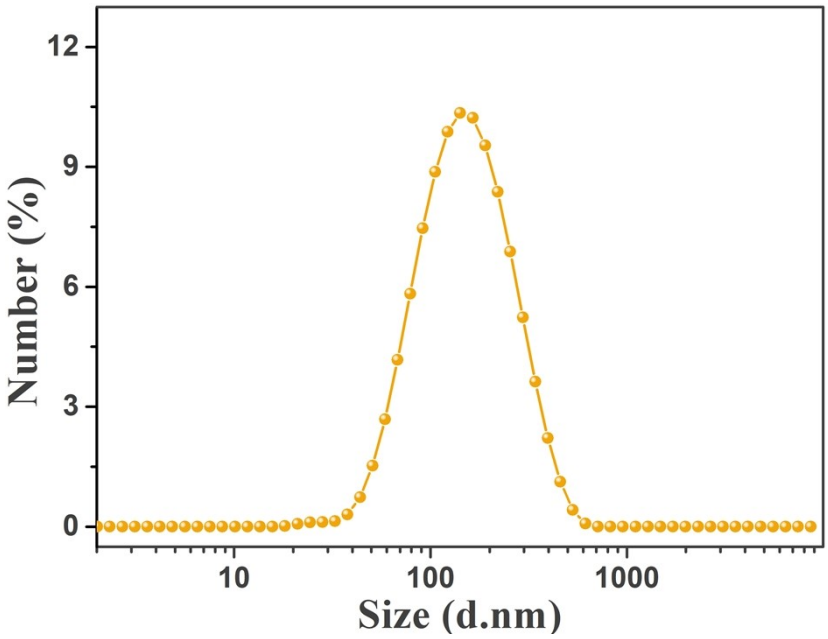

Figure S2. DLS spectra of PFGA-$CsPbBr_3$ NCs.

Figure S3. Photograph show the PFGA-$CsPbBr_3$ NCs in different solvents, including n-hexane, toluene, ethyl acetate, acetone, tert-butanol, isopropanol, ethanol, acetonitrile, from left to right under normal white light (up) and a 365 nm UV (down).

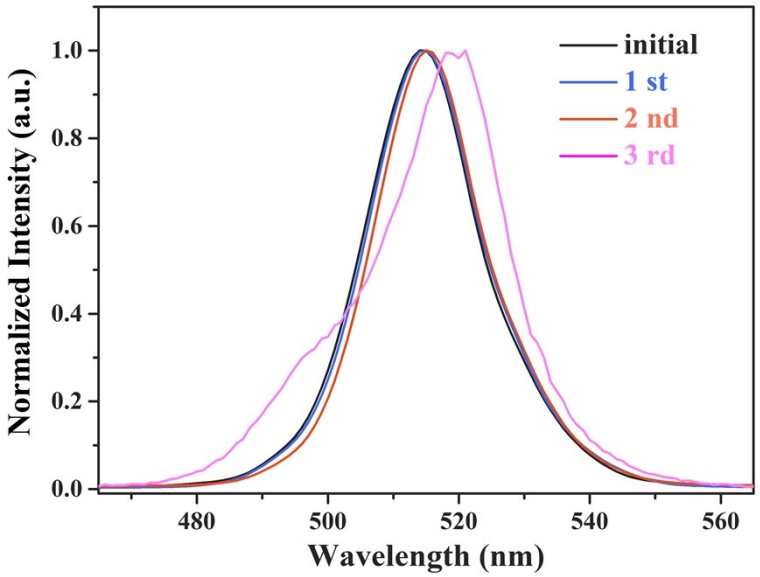

Figure S4. Purification and washing stability of OA/OAm-capped $CsPbBr_3$ NCs with toluene.

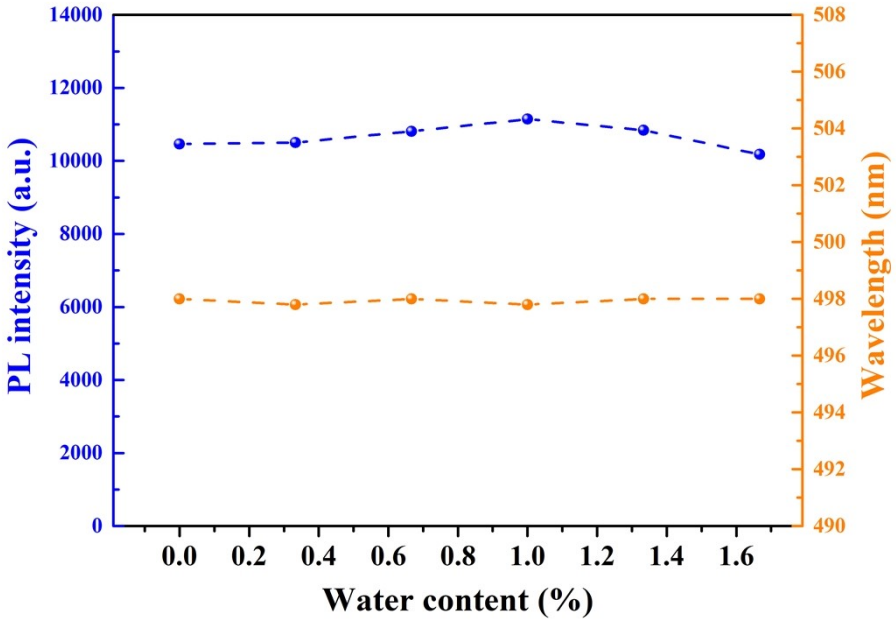

Figure S5. The relative PL intensity (blue line) and their PL peak wavelength (orange line) of the PFGA-$CsPbBr_3$ NCs ethanol solution reacting with H_2O of different concentration.

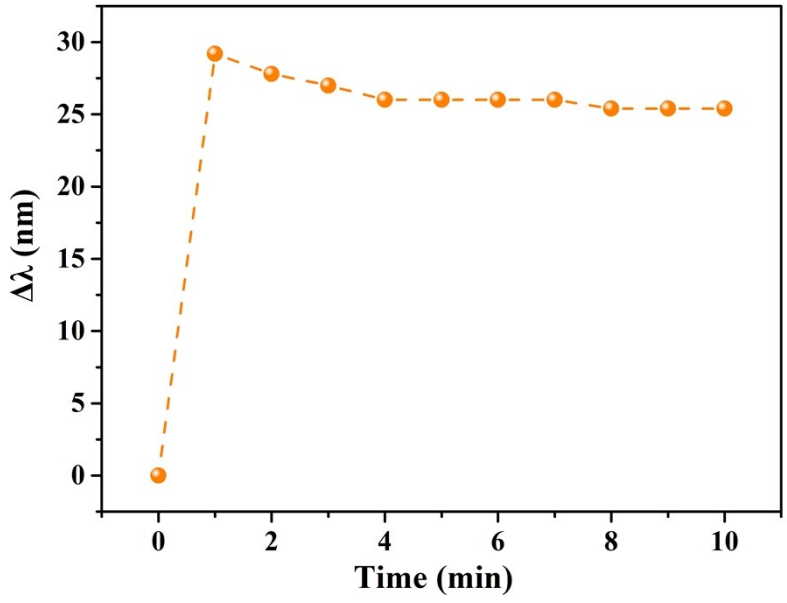

Figure S6. The wavelength changes of PFGA-$CsPbBr_3$ NCs solution with 120 mmol/L NaCl at different time.

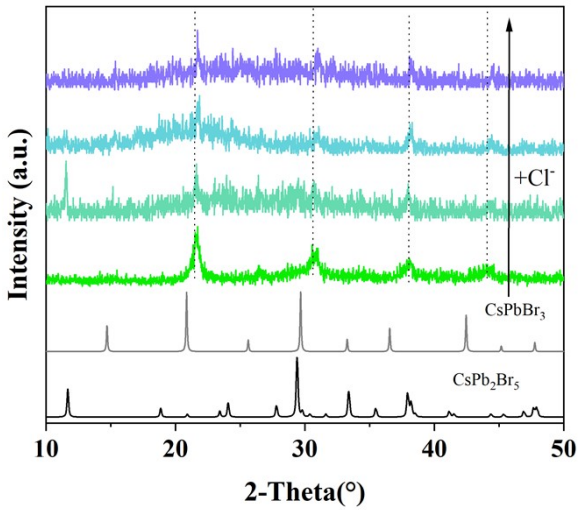

Figure S7. The XRD patterns of PFGA-$CsPbBr_3$ PNCs after addition of Cl^-

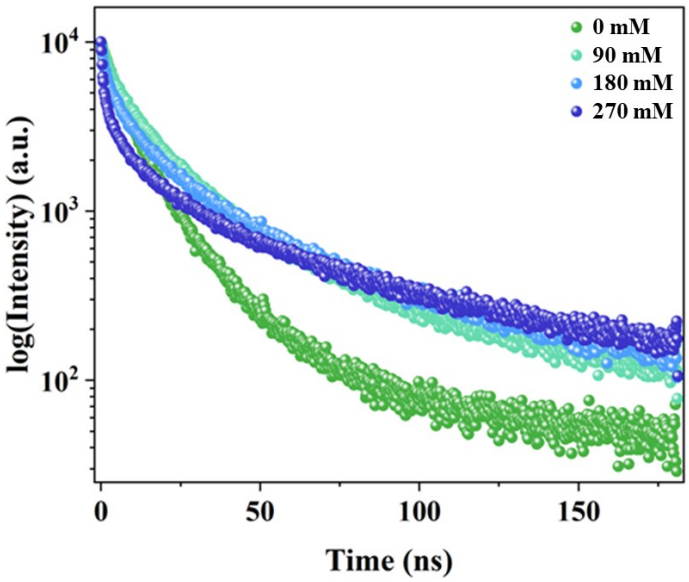

Figure S8. The PL lifetime changes of $CsPbBr_3$ PNCs after halide exchange

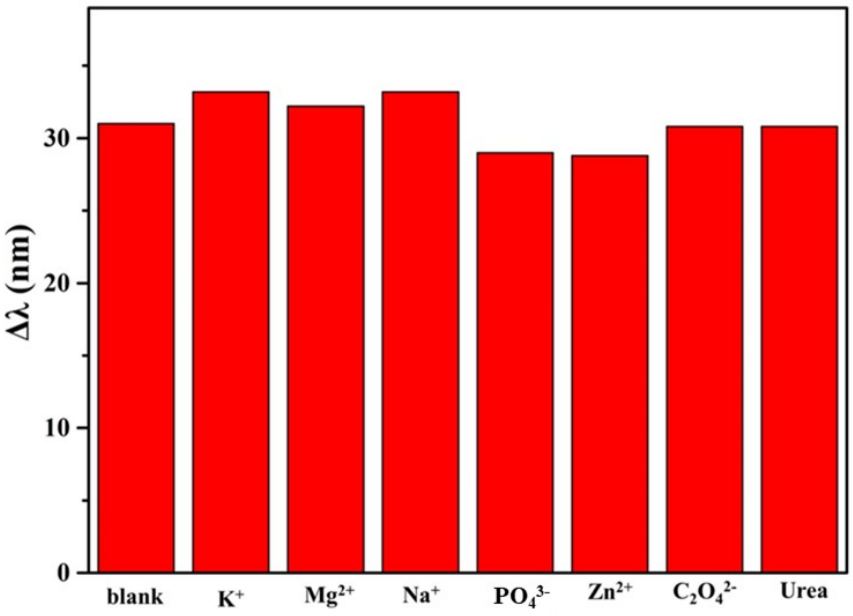

Figure S9. The selectivity investigation in urine based on PFGA-$CsPbBr_3$ NCs halide exchanges with Cl^- (120 mmol/L). The coexistent in urea from left to right were 60 mmol/L K^+, 2 mmol/L Mg^{2+}, 130 mmol/L Na^+, 0.8 g/L PO_4^{3-}, 9 μmol/L Zn^{2+}, 200 μmol/L $C_2O_4^{2-}$ and 180 μmol/L urea.

Table S1. Atomic structure of optimized $CsPbBr_3$ (001) surface with PFVA/PGSA/ PFGA/PFAA molecule and their calculation results

Ligand	PFVA	PFSA	PFGA	PFAA
Structural formula	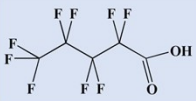	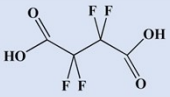	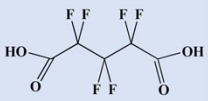	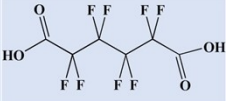
Atomic structural of optimized $CsPbBr_3$ (001)	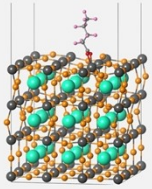	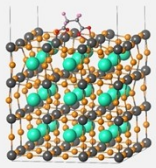	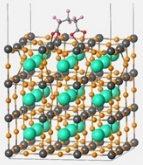	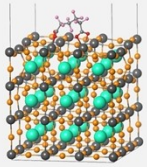
Optimized molecular radial length		5.17 Å	6.33 Å	7.75 Å
Spacing in Pb^{2+}-Pb^{2+}	6.02 Å			
Binding energy	-1.42 eV	-4.83 eV	-5.19 eV	-3.98 eV

Table S2. Ligands for the synthesis of $CsPbX_3$ NCs

Sample	*Surface Ligands*	*PLQY*	*Stability (test time and dispersion solvent)*	*Publication*	*Ref.*
$CsPbX_3$	OA/OAm	50-90%		2015	[10]
$CsPbBr_3$	OA	70%	14 days in toluene	2016	[11]
$CsPbI_3$	OAm/TMPPA	90%	20 days in hexane	2017	[12]
$CsPbI_3$	OAm/IDA	95%	15 days in n-hexane	2018	[13]
$CsPbBr_3$	Zwitterionic	90%	28 days in toluene	2018	[14]
$CsPbBr_3$	OA/OPA	90%	20 min in hexane (2.4 vol% ethanol)	2018	[15]
$CsPbBr_3$	1,4-DBSA	95%	5 months in toluene	2018	[16]
$CsPbBr_3$	OA/OAm/ X-type ligands	~100%		2018	[17]
$CsPbBr_3$	L-Type Ligand	~100%		2019	[18]
$CsPbBr_3$	OA/OAm/ DDDMAB	~100%	3 weeks in n-hexane	2019	[19]
$CsPbBr_3$	$PbBr_2$-adlayers/ DDAB		6 h in hexane (20 vol% ethanol)	2019	[20]
$CsPbBr_3$	PDB	80%	24 h in hexane (50 vol% ethanol)	2019	[21]
$CsPbBr_3$	OA/St^-/TOPO		30 days in ethanol	2020	[22]
$CsPbBr_3$	$DC_{12}AB$-$PbBr_2$	83.9%	60 days in toluene	2020	[23]
$CsPbI_3$	OA/OAm/ DDAB	90%	60 days in n-hexane	2020	[24]
$CsPbBr_3$	OA/OLA	91.3%	5 weeks in n-hexane	2020	[25]
$CsPbBr_3$	DBSA/DDAB	97%	90 days in toluene	2021	[26]
$CsPbBr_3$	GA	38.1%	15 days in ethanol gel	2021	[27]
$CsPbBr_3$	α-PVDF	98%	60 days in toluene	2021	[28]
$CsPbBr_3$	OAm/BDGA	~100%	60 days in toluene	2022	[29]
$CsPbBr_3$	OAm/BBA	86.4%	4 days in water	2022	[30]
$CsPbBr_3$	OMPA	80.13	15 days in water	2022	[31]

$CsPbBr_3$	PFGA	86%	60 days in ethanol		This work

Note: Oleic acid (OA), oleamine (OAm), bis-(2, 2, 4-trimethylpentyl) phosphinic acid (TMPPA), 2, 2′-iminodibenzoic acid (IDA), long-chain zwitterionic molecules including 3-(N, N-dimethyloctadecylammonio) propanesulfonate, N-hexadecylphosphocholine, or N, N-dimethyldodecylammoniumbutyrate, Octylphosphonic acid (OPA), 1,4-Dodecyl benzene sulfonic acid (1,4-DBSA), X-type ligands including benzoate, difluoroacetate, or hexylphosphonate, L-type ligands including OAm, n-octylamine or undecylamine; didodecyl dimethylammonium bromide (DDDMAB), didodecyldimethylammonium bromide (DDAB), n-propyltrimethoxysilane-dimethyloctadecylammonium bromine (PDB), stearic acid (St^-), trioctyl-phosphine oxide (TOPO), didodecyldimethylammonium bromide ($DC_{12}AB$), octylamine (OLA), glycyrrhizic acid (GA), α-polyvinylidene fluoride (α-PVDF), Boc-D-glutamic acid (BDGA), 4-bromo-butyric acid (BBA), octylamine-modified polyacrylic acid (OMPA).

Table S3. The results for Cl^- detection in the urine

Samples	Average found (mM, n=3)	Cl^- add (mM)	Cl^- found (mM)	Recovery (%)	RSD (%) (n=3)
urine 1	131.3	30	30.3	101	1.9
urine 2	158.2	30	32	106	1.8
urine 3	91.9	30	28.3	94	2.3

Table S4. Comparation of chloride sensing in different solvents

Type of detection	**Solvent**	**Detection time**	**Ligands**	**Ref.**
Heterogeneous detection	n-hexane/water	5 min	St/OAm	[32]
Homogeneous detection	water	5 min	OMPA	[31]
Homogeneous	ehanol/water	~1 s	GA	[33]

detection				
Homogeneous detection	ehanol/water	20 s	PFGA	This work

References

1. X. Li, Y. Wu, S. Zhang, B. Cai, Y. Gu, J. Song, H. Zeng, *Adv. Funct. Mater.,* 2016**, 26**, 2435-2445.
2. L. Protesescu, S. Yakunin, M. I. Bodnarchuk, F. Krieg, R. Caputo, C. H. Hendon, R. X. Yang, A. Walsh, M. V. Kovalenko, *Nano Lett.,* 2015, **15**, 3692-3696.
3. T. D. Kühne, M. Iannuzzi, M. Del Ben, V. V. Rybkin, P. Seewald, F. Stein, T. Laino, R. Z. Khaliullin, O. Schütt, F. Schiffmann, D. Golze, J. Wilhelm, S. Chulkov, M. H. Bani-Hashemian, V. Weber, U. Borštnik, M. Taillefumier, A. S. Jakobovits, A. Lazzaro, H. Pabst, T. Müller, R. Schade, M. Guidon, S. Andermatt, N. Holmberg, G. K. Schenter, A. Hehn, A. Bussy, F. Belleflamme, G. Tabacchi, A. Glöß, M. Lass, I. Bethune, C. J. Mundy, C. Plessl, M. Watkins, J. VandeVondele, M. Krack, J. Hutter, *J. Chem. Phys.,* 2020, **152**, 194103.
4. S. Goedecker, M. Teter, J. Hutter, *Phys. Rev. B.,* 1996, **54**, 1703.
5. J. VandeVondele, J. Hutter, *J. Chem. Phys.,* 2007, **127**, 114105.
6. J. P. Perdew, K. Burke, M. Ernzerhof, *Phys. Rev. Lett.,* 1996, **77**, 3865-3868.
7. S. Grimme, S. Ehrlich, L. Goerigk, *J Comput Chem.,* 2011**, 32**, 1456-1465.
8. S. Grimme, J. Antony, S. Ehrlich, H. Krieg, *J. Chem. Phys.,* 2010**, 132**, 154104.
9. S. F. Boys, F. Bernardi, *Mol Phys.,* 1970**, 19**, 553-566.
10. L. Protesescu, S. Yakunin, M. I. Bodnarchuk, F. Krieg, R. Caputo, C. H. Hendon, R. X. Yang, A. Walsh, M. V. Kovalenko, *Nano Lett.,* 2015, **15**, 3692-3696.
11. E. Yassitepe, Z. Yang, O. Voznyy, Y. Kim, G. Walters, J. A. Castañeda, P. Kanjanaboos, M. Yuan, X. Gong, F. Fan, J. Pan, S. Hoogland, R. Comin, O. M. Bakr, L. A. Padilha, A. F. Nogueira, E. H. Sargent, *Adv. Funct. Mater.,* 2016, **26** (47), 8757-8763.
12. C. Wang, A. S. R. Chesman, J. J. Jasieniak, *Chem. Commun.,* 2017, **53**, 232-235.
13. J. Pan, Y. Shang, J. Yin, M. D. Bastiani, W. Peng, I. Dursun, L. Sinatra, A. M. El-Zohry, M. N. Hedhili, A. H. Emwas, O. F. Mohammed, Z. Ning, O. M. Bakr, *J. Am. Chem. Soc.,* 2018, **140**, 562-565.
14. F. Krieg, S. T. Ochsenbein, S. Yakunin, S. ten Brinck, P. Aellen, A. Süess, B. Clerc, D. Guggisberg, O. Nazarenko, Y. Shynkarenko, S. Kumar, C.-J. Shih, I. Infante, M. V. Kovalenko, *ACS Energy Lett.,* 2018, **3**, 641-646.
15. Y. Tan, Y. Zou, L. Wu, Q. Huang, D. Yang, M. Chen, M. Ban, C. Wu, T. Wu, S. Bai, T. Song, Q. Zhang, B. Sun, *ACS Appl. Mater. Interfaces.,* 2018, **10**, 3784-3792.
16. D. Yang, X. Li, W. Zhou, S. Zhang, C. Meng, Y. Wu, Y. Wang, H. Zeng, *Adv. Mater.,* 2019, **31**, 1900767.
17. D. P. Nenon, K. Pressler, J. Kang, B. A. Koscher, J. H. Olshansky, J, H. Olshansky, *J. Am. Chem. Soc*. 2018, **140**, 50, 17760-17772.
18. Q. X. Zhong, M. Cao, Y. F. Xu, P. L. Li, Y. Zhang, H. C. Hu, D. Yang, Y. Xu, L. Wang, Y. Y. Li, X. H. Zhang, Q. Zhang, *Nano Lett.,* 2019, **19**, 6, 4151-4157.

19. M. Imran, P. Ijaz, L. Goldoni, D. Maggioni, U. Petralanda, M. Prato, G. Almeida, I. Infante, L. Manna, *ACS Energy Lett.*, 2019, **4** (4), 819-824.
20. L. J. Ruan, B. Tang, Y. Ma, *J. Phys. Chem. C*, 2019, **123** (18), 11959-11967.
21. Q. Xie, D. Wu, X. Wang, Y. Li, *J. Mater. Chem. C,* 2019, **7** (36), 11251-11257.
22. Y. X. Liu, D. Li, L. L. Zhang, Y. Chen, C. Geng, S. Shi, Z. Zhang, W. Bi, S. Xu, *Chem. Mater.,* 2020, **32**, 1904-1913.
23. T. Chiba, Y. Takahashi, J. Sato, S. Ishikawa, H. Ebe, K. Tamura, S. Ohisa, J. Kido, *ACS Appl. Mater. Interfaces,* 2020, **12**, 45574-45581.
24. Y. H. Huang, W. L. Luan, M. K. Liu, L. Turyansk, *J. Mater. Chem. C*, 2020, **8**, 2381-2387.
25. Q. Xiong, S. Huang, J. Du, X. Tang, F. Zeng, Z. Liu, Z. Zhang, T. Shi, J. Yang, D. Wu, H. Lin, Z. Luo, Y. Leng, *Adv. Opt. Mater.,* 2020, **8**, 2000977.
26. L. Zheng, K. Jiang, X. Li, P. Hong, K. Chen, H. Zhang, Y. Song, B. Luo, *J. Colloid. Interf. Sci.,* 2021, **598**, 166-171.
27. L. L. Zheng, K. Y. Jiang, X. L. Li, P. B. Hong, K. Chen, H. Zhang, Y. B. Song, B. B. Luo, J. *Colloid Interface Sci.*, 2021, **598**, 166-171.
28. L. Yang, B. Fu, X. Li, H. Chen, L. Li, *J. Mater. Chem. C,* 2021, **9**, 1983-1991.
29. Y. Zhang, G. Li, G. Hou, J. Lin, M. Chen, S. Liu, H. Lin, J. Fang, C. Jing, J. Chu, *Chem. Eng. J.,* 2022, **438**, 135270.
30. H. Zhu, Y. Pan, C. Peng, H. Lian, J. Lin, *Angew. Chem. Int. Ed.,* 2022, **61**, e202116702.
31. Y. Shu, Y. Wang, J. Guan, Z. Ji, Z. P. Ji, Q. Xu, X. Y. Hu, *Anal. Chem.* 2022, **94**, 5415–5424.
32. F. M. Li, Y. F. Feng, Y. P. Huang, Q. H. Yao, G. H. Huang, Y. M. Zhu, X. Chen, *Microchimica Acta*, 2021, **188**, 2-8.
33. X. L. Li, J. Li, P. B. Hong, W. X. Ni, B. B. Luo, *Anal. Methods*, 2023, **15**, 2318-2325.